

THE SEQUENCE-OF-BIFURCATIONS APPROACH TOWARDS UNDERSTANDING TURBULENT FLUID FLOW

F. H. BUSSE

*Institute of Physics, University of Bayreuth, D-95447 Bayreuth, Germany
E-mail: busse@uni-bayreuth.de*

(Received 19 September 2002; accepted 30 April 2003)

Abstract. The sequence-of-bifurcations approach for the analysis of transitions from simple to complex forms of fluid flow is described. Formulated for fluid systems with external conditions that are homogeneous in two spatial dimensions and in time, this approach determines bifurcations through their symmetry breaking properties. Solutions that are periodic in the homogeneous dimensions and in time are generated in this way. While the secondary solution induced by the instability of the basic homogeneous state generically assumes the form of rolls or stripes, higher bifurcations introduce solutions exhibiting structures specific for the physical system under consideration. These structures often persist in the form of coherent structures in the turbulent state of the system. Examples from the case of thermal convection in a layer heated from below are used to illustrate the sequence-of-bifurcations approach.

Keywords: bifurcation, bimodal cells, coherent structures, knot convection, oscillatory bimodal convection, Rayleigh-Bénard convection, symmetry breaking, thermal convection, turbulence

1. Introduction

Most efforts directed towards an improved understanding of turbulent fluid flow are based on statistical analysis. Since the details of the nearly random velocity fields observed in laboratory experiments or in numerical simulations are of little interest one usually tries to characterize turbulent systems by their statistical properties and by their time averaged properties in particular. Since it is generally believed that the basic Navier–Stokes equations (NSE) of motion provide the correct basis for the description of turbulent fluid flow it is regrettable that rather little information from the basic dynamical balances enters into the statistical analysis of turbulence. Of course, fluid dynamicists are well aware of coherent structures that are observed in turbulent fluid motions, and often these structures can be related to the form of instabilities of a basic laminar state as, for example, in the case of the mixing layer (Brown and Roshko, 1974). But there are few more systematic attempts to relate typical spatial or temporal coherent features of turbulence to solutions of the NSE.

The goal of this paper is to demonstrate that relatively simple solutions of the basic Navier–Stokes equations of motion can be quite useful for the understanding of typical dynamical mechanisms operating in turbulent fluid systems. While the spatially and temporally periodic solutions of the NSE do not exhibit the chaotic



nature of realized turbulence they may well exhibit the same transport mechanism that also operates under turbulent conditions at similar high values of the control parameter. These “regular” solutions as we shall call them, in distinction to the turbulent solutions, may well be unstable and thus not observable in experiments. But there are many situations where regular solutions are stable with respect to infinitesimal disturbances and where their basins of attraction in the solution space are just too small to provide them with a chance to be realized in an experiment. Only if controlled initial conditions are used in experiments is it possible to enter the appropriate basins of attraction and to realize a regular state at external conditions which ordinarily give rise to a turbulent state.

The idea of considering regular solutions instead of turbulent states at given external conditions requires the restriction to systems that are homogeneous with respect to at least one dimension in space or in time. Among the manifold of regular solutions only those which are stable with respect to infinitesimal disturbances within a prescribed periodicity interval are of physical interest. In order to make an optimal use of the virtual world of “stable” regular solutions we shall focus on problems with the maximum number of two homogeneous spatial dimensions and we shall also require homogeneity in time as, for instance, in the case of constant external conditions. Since we are considering non-equilibrium systems there must always be a dimension in which an energy flux enters and exits the system. Fortunately, these limitations are not overly restrictive since physicists, applied mathematicians and engineers have traditionally studied fluid dynamical problems in their simplest forms which often correspond to a homogeneous configuration. In the following we shall first point out some typical examples in Section 2 and then consider secondary solutions in the form of rolls and their instabilities in Section 3. Three-dimensional solutions evolving from secondary and higher order bifurcations are described in Section 4. In Section 5 examples drawn from the problem of convection in a layer heated from below are discussed in some detail. The paper closes with a more general discussion.

2. Fluid Systems that are Homogeneous in Two Dimensions

In Figure 1 some typical systems are displayed which are characterized by two homogeneous dimensions and steady external conditions. But there are many other systems which have not been shown in the figure for a lack of space. For example, a spherical fluid shell heated from within and subject to a spherically symmetric distribution of gravity is homogeneous with respect to two dimensions and is inhomogeneous only with respect to the radial coordinate. While the basic state or primary solution reflects the homogeneity of the configuration of the problem, spontaneous symmetry breakings characterize the solutions bifurcating from the basic state as the control parameter increases. Unless the bifurcation is subcritical these bifurcating solutions can usually be realized in experiments when a suffi-

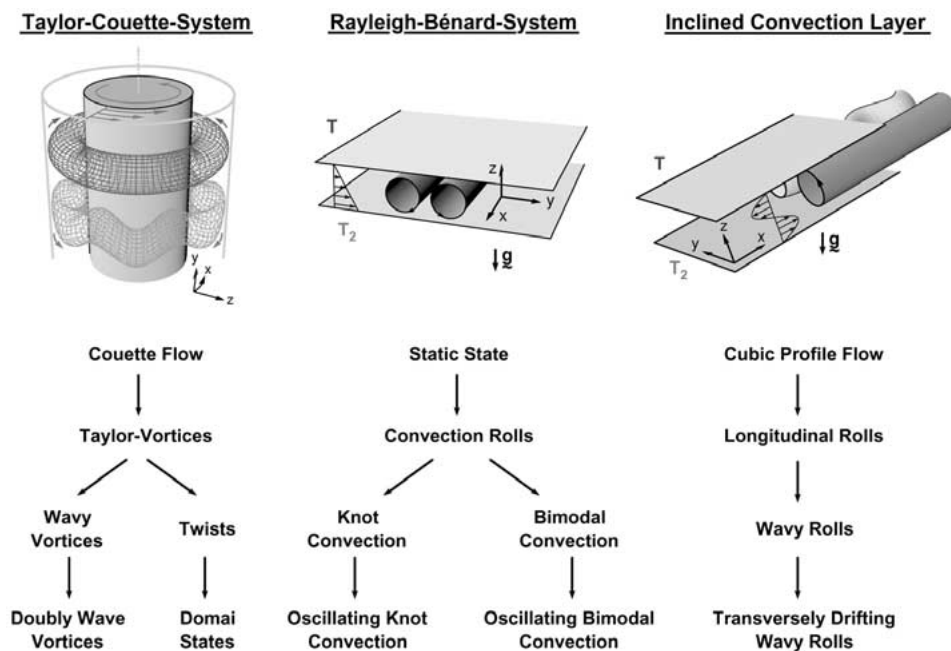


Figure 1. Examples for sequences of bifurcations in fluid dynamical systems.

ciently good approximation for homogeneity is used. The bifurcating solution can be steady or oscillatory, but it is typically two-dimensional, i.e. it assumes the form of rolls or stripes. With further increasing control parameter secondary bifurcations are likely to occur which will break additional symmetries by introducing, for instance, a second spontaneous wavenumber along the axis of the rolls.

While the secondary solution introduced by the first bifurcation is rather similar in all cases owing to its two-dimensional nature, the tertiary, quaternary and higher order states introduced by the second, third and higher bifurcations are specific to the respective problems and may also change depending on the additional parameters for a given problem. For this reason different branches of bifurcation sequences have been indicated in Figure 1 in the cases of the Taylor-Couette-system and the Rayleigh-Bénard layer. Further branches exist which have not been mentioned. The approach to be described in the following has been developed to follow these bifurcation branches and to identify the physical mechanisms that are the cause of the bifurcations.

Before we consider the mathematical method let us summarize the main points of the approach:

- In many cases the reduction of inhomogeneity to a single spatial dimension presents a dynamical mechanism in its simplest form.
- Homogeneity in two spatial dimensions and in time maximizes the symmetries the breaking of which permits the identification of bifurcations.

- A homogeneous formulation of a problem also simplifies the numerical analysis. Symmetries reduce the number of degrees of freedom that must be taken into account.
- While exact homogeneity is usually not realized in nature nor in laboratory experiments, the bifurcations of the ideal system typically become only slightly imperfect bifurcations as long as the deviations from homogeneity are sufficiently small and the dimensions of the system are large compared to typical wavelengths associated with the bifurcations.
- The spatially and time periodic solutions represent only a tiny fraction of the realizable manifold of solutions of the basic equations. Even if the periodic solutions are stable with respect to infinitesimal disturbances, their basins of attraction are usually small and tend to decrease in size with increasing control parameter. The dynamical structures observed in nature or in the laboratory are thus typically more irregular and may have a chaotic time dependence. Nevertheless the regular periodic solutions deserve special attention since they exhibit most clearly the dynamical properties of the flow and their changes with increasing control parameter.

3. Mathematical Description of Secondary Solutions and their Instabilities

In keeping with the general character of the sequence-of-bifurcations approach we shall not consider specific equations here. Instead we consider the more abstract mathematical problem of the form

$$\underline{L}X + R\underline{K}X - \underline{M}\frac{\partial}{\partial t}X = \underline{N}(X, X) \quad (1)$$

where the vector valued variable X describes the deviation from the basic state which exhibits the same degree of homogeneity as the external conditions of the system. For this reason Equation (1) is homogeneous and homogeneous boundary conditions must be obeyed by X in the inhomogeneous direction of the system. \underline{L} , \underline{K} , \underline{M} are linear operators involving partial derivatives, while $\underline{N}(X, X)$ is the nonlinear part which typically is quadratic in the variable X . R denotes a control parameter such as the Rayleigh or Reynolds number. Although the surfaces of homogeneity could be spherical or cylindrical for simplicity we shall restrict the attention to planar surfaces. Accordingly we introduce a Cartesian system of coordinates x, y, z with the z -coordinate in the inhomogeneous dimension. The operators of Equation (1) may thus depend on z , but not on x, y or time t . In the analogous problems with cylindrical or spherical symmetry the radial coordinate assumes the role of the z -coordinate.

In order to investigate the stability of the basic state with respect to infinitesimal disturbances we neglect the right hand side of Equation (1) and look for solutions of the general form

$$\mathbf{X} = \exp\{i\mathbf{l} \cdot \mathbf{r} + \sigma t\} \mathbf{G}(\mathbf{l}, z) \quad (2)$$

where \mathbf{l} is an arbitrary wavevector parallel to the surfaces of homogeneity and σ is the growth rate which represents the complex eigenvalue of the linear homogeneous Equation (1) with vanishing right hand side. Of physical interest is the lowest value of R for which an eigenvalue σ exists as a function of \mathbf{l} with vanishing real part σ_r . The corresponding values R_c of R and \mathbf{l}_c of \mathbf{l} are called critical control parameter and critical wave vector, respectively. If the imaginary part σ_i of σ is finite it is called critical frequency. For R exceeding R_c disturbances of the form (2) will grow, but their amplitudes will saturate owing to the action of the nonlinearity on the right hand side of Equation (1) which can no longer be neglected at a finite amplitude of \mathbf{X} . In the case of a supercritical bifurcation, which we shall assume, the saturated amplitude varies smoothly with $R - R_c$. For the description of this solution we orientate the coordinate system such that y points in the direction of \mathbf{l}_c and assume $\sigma_i = 0$. The treatment of the case $\sigma_i \neq 0$ is analogous though slightly more complex. We thus arrive at the representation

$$X_i = \sum_{m,n} a_{mn}^{(i)} \exp\{im\alpha y\} G_n^{(i)}(z) \quad (3)$$

for the steady bifurcating solution in the form of rolls or stripes. The vector functions $G_n^{(i)}$ denote a complete system satisfying all boundary conditions and the wavenumber α typically is set equal to $|\mathbf{l}_c|$. But when R exceeds R_c there usually exists a neighborhood of wavevectors \mathbf{l} around \mathbf{l}_c for which solutions of the form (3) can be obtained.

The two-dimensional solution (3) bifurcating at the point of instability of the primary state represents the generic case of the secondary solution. But other solutions may be found in special cases when additional symmetries exist. If there exist, for example, two wavevectors, \mathbf{l}_1 and \mathbf{l}_2 , which correspond to the critical conditions, then more complex three-dimensional solutions fitting the lattice spanned by the two wavevectors may be possible. If the system is not only homogeneous but also isotropic, as in the case of a horizontal Rayleigh-Bénard fluid layer heated from below, then an infinite degeneracy occurs in that all wavevectors \mathbf{l} with the same absolute value, $|\mathbf{l}| = \alpha_c$, are equivalent. Figure 2 demonstrates the considerable difference between the isotropic case and the generic homogeneous case. A detailed analysis of Rayleigh-Bénard convection (Schlüter et al., 1965) shows that solutions in the form of rolls are preferred if the Boussinesq approximation can be assumed. Deviations from the Boussinesq approximation cause the appearance of hexagonal convection cells at onset. But these are replaced by rolls as the Rayleigh number increases when those deviations are not too large (Busse, 1967a). Thus we

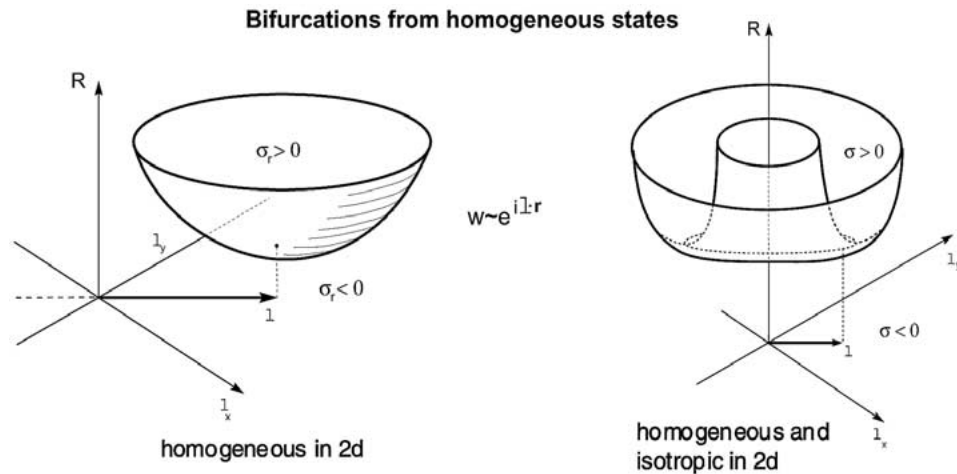


Figure 2. Onset of instability in a generic homogeneous system (left) and in the special case of an isotropic system (right).

can conclude that even in the case of Rayleigh-Bénard convection rolls of the form (3) can be assumed as secondary solution.

Although solutions of the form (3) are likely to exist for all values $R > R_c$, they will in general become unstable as R increases much beyond R_c . In order to investigate the stability with respect to infinitesimal disturbances \tilde{X} we must solve the linear homogeneous problem

$$\underline{L}\tilde{X} + R\underline{M}\tilde{X} + \underline{V}\frac{\partial}{\partial t}\tilde{X} = N(\tilde{X}, X) + N(X, \tilde{X}) \tag{4}$$

Since X is steady and periodic in y a Floquet ansatz

$$\tilde{X}_i = \exp\{ibx + idy + \sigma t\} \sum_{m,n} \tilde{a}_{nm}^{(i)} \exp\{im\alpha y\} G_n^{(i)}(z) \tag{5}$$

can be assumed without losing generality. For a given solution of the form (3) the eigenvalues σ must be determined depending on the wavenumbers b and d . Whenever there exists a σ with positive real part σ_r , the steady roll solution X is unstable. If all σ_r are negative or zero the solution X is regarded as stable. There always exists the neutral disturbance $\tilde{X} = \partial X / \partial y$ as a solution of Equation (4) with $\sigma = 0$ which corresponds to an infinitesimal translation of the steady roll solution perpendicular to its axis. In order to classify the growing disturbances of the form (5) it is convenient to consider all symmetries of the solution (3) which could possibly be broken by the instability. Among the symmetries of rolls listed in Table I the first three are common to all solutions of the form (3). The additional symmetry D is found for convection rolls in a Rayleigh-Bénard layer or for Taylor vortices between differentially rotating cylinders. In the limit when

TABLE I

Symmetry properties of two-dimensional rolls (w refers to the velocity component in the z -direction)

A	Translation in time:	$\partial w / \partial t = 0$
B	Translation along roll axis:	$\partial w / \partial x = 0$
C	Transverse periodicity:	$w(y + 2\pi / \alpha_1 z) = w(y, z)$
D	Transverse reflection:	$w(-y, z) = w(y, z)$ or $a_{-mn} = a_{mn}$
E	Inversion about roll axis:	$w(y + \frac{\pi}{\alpha}, z) = -w(y, -z)$ or $a_{mn} = 0$ for odd $m + n$

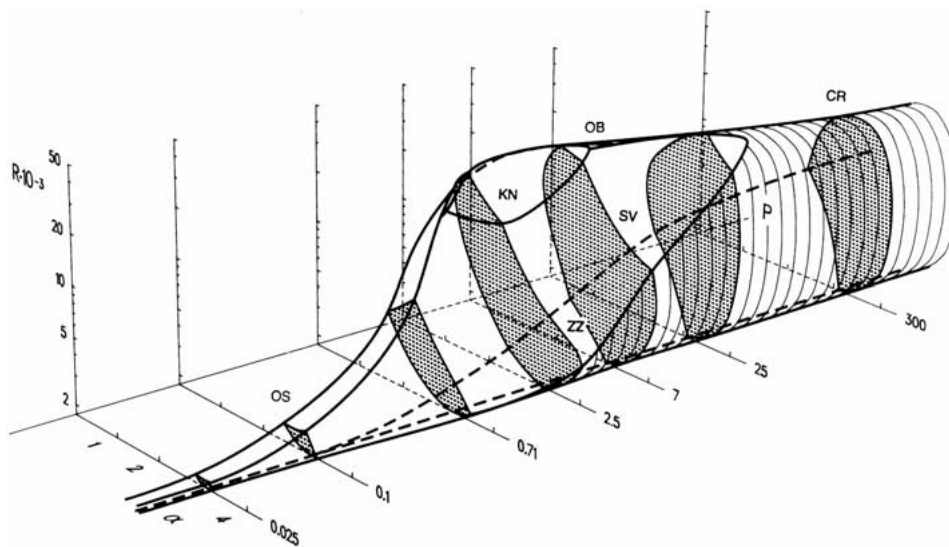


Figure 3. Region of stable convection rolls in a Ra - α - Pr -parameter space. The region of stable rolls is bounded by surfaces corresponding to the onset of the instabilities listed in Table II. Note that the Prandtl number Pr corresponds to P in the figure increasing towards the right and R corresponds to Ra . The symbols CR, ... indicate the onset of the respective instabilities as listed in Table II.

the gap between the two cylinders becomes small and the rotation rate becomes nearly equal the fifth symmetry property E also holds for Taylor vortices. In the Rayleigh-Bénard case symmetry E holds if the layer is symmetric with respect to its mid plane.

In Table II typical instabilities of rolls are listed that have been found in the Rayleigh-Bénard case and in other systems. For details we refer to the papers by Busse (1967b), Clever and Busse (1974), Busse and Clever (1979), Bolton and Busse (1985) and Bolton et al. (1986). An impression of the way in which the instabilities of Table II restrict the domain of stable rolls in the Ra - α - Pr -parameter

TABLE II
Symmetries Broken by Bifurcations from Rolls

Broken Symmetries	A	B	C	D	E	Remarks
Properties of disturbances	$\sigma_i \neq 0$	$b \neq 0$	$d \neq 0$	$\tilde{a}_{mm} \neq \tilde{a}_{-mn}$	$\tilde{a}_{mm} \neq 0$ for $m+n = \text{odd}$	
Eckhaus Instab.			X	X		
Crossroll Instab.	CR	X			X) differ by value of b
Knot-Instability	KN	X			X	
Even Blob-Instab.	EB	X				
Odd Blob-Instab.	OB	X			X	
Oscillatory Instab.	OS	X		X		occurs also as wavy in- stability of Taylor vortices
Zig-Zag-Instability	ZZ	X		X		
Skewed Varicose Instab. SV		X	X	X		occurs as Küppers-Lortz instability in a rotating convection layer
Osc. Skewed Var. Inst.		X	X	X		

space can be gained from Figure 3. Here Ra is the Rayleigh number and Pr is the Prandtl number which is defined as the ratio between the kinematic viscosity and thermal diffusivity, $Pr = \nu/\kappa$. Some of the instabilities listed in Table II do not lead to new states of convection, but instead they lead to convection rolls with different wavelengths corresponding to values of α in the stable domain, as, for example, in the case of the Eckhaus instability or in the case of the cross roll instability at lower values of the Rayleigh number. Of special interest, however, are those instabilities which evolve into three-dimensional structures. These latter are called tertiary solutions and will be considered in the next section.

4. Three-Dimensional Solutions Emerging from Secondary and Higher-Order Bifurcations

Although not all instabilities listed in Table II lead to the development of new three-dimensional forms of convection most of them do, at least in some region of the parameter space. For example, the cross-roll instability initiates the growth of rolls at right angles to the given roll structure. At Rayleigh numbers not too far above the critical value the growth of the perpendicular rolls and the concurrent decay of the original rolls go all the way until the original rolls with their too short wavelength are replaced by the perpendicular or cross-rolls with a wavenumber close to the critical value (Busse and Whitehead, 1971). But at high Rayleigh numbers of the order of 2×10^4 the cross-roll instability is actually characterized by a value of the wavenumber b much larger than the critical value α_c and thus can not just lead to a replacement of the given roll pattern by a more stable one. Instead a steady boundary layer type structure develops as indicated in Figure 4 and the evolution of the cross-roll instability thus leads to the new form of bimodal convection. Since the secondary set of rolls has a smaller wavelength it is especially suited to increase the heat transport in the thermal boundary layers. In this way bimodal convection is more efficient in transporting heat than two-dimensional rolls (Frick et al., 1983).

The physical origin of the transition to bimodal convection can most easily be understood through a consideration of the stability of the thermal boundary layers as indicated in Figure 5. Convection gives rise to a nearly constant horizontally averaged temperature in the interior of the layer. But the heat transport can be carried only by conduction across the boundary. Since the velocity vanishes near the rigid boundaries, the same Rayleigh criterion for the instability of a static fluid layer heated from below may be applied to the thermal boundary layers

$$\frac{1}{2}Ra\delta^3 > Ra_c \quad \text{for instability.} \quad (6)$$

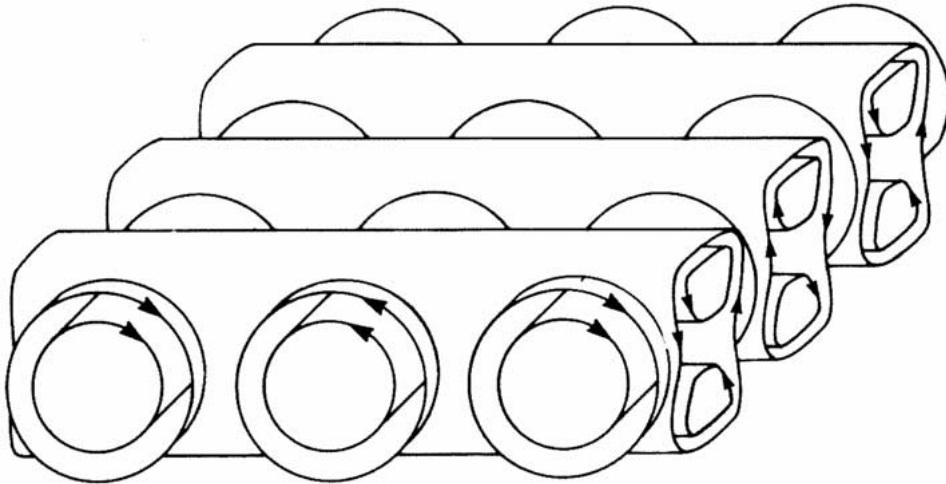


Figure 4. Schematic sketch of bimodal convection in a fluid layer heated from below.

where the factor $\frac{1}{2}$ indicates that half of the temperature difference ($T_2 - T_1$) decreases across the thermal boundary layer and where the factor δ^3 enters because the definition of the Rayleigh number

$$Ra = \frac{\gamma(T_2 - T_1)gd^3}{\nu\kappa} \quad (7)$$

depends on third power of the thickness d of the respective layer. Here γ denotes the coefficient of thermal expansion of the fluid. The ratio δ between the thickness of the thermal boundary layers and the thickness of the entire layer can be expressed by the Nusselt number, which is the ratio between the total heat flux and that carried by conduction in the absence of convection,

$$Nu = \frac{1}{2\delta} \quad (8)$$

Accordingly the criterion (6) for instability of the thermal boundary layers can be written in the form

$$Nu < \left(\frac{Ra}{16Ra_c} \right)^{\frac{1}{3}} \text{ for instability} \quad (9)$$

Since convection rolls are not capable of attaining a sufficiently strong growth of Nu with the Rayleigh number Ra in the presence of rigid boundaries they must become unstable.

Another way in which instabilities may lead to a more efficient convective heat transport is presented by the knot instability. This instability breaks the same symmetries as the cross-roll instability, but does so with a much smaller value of the

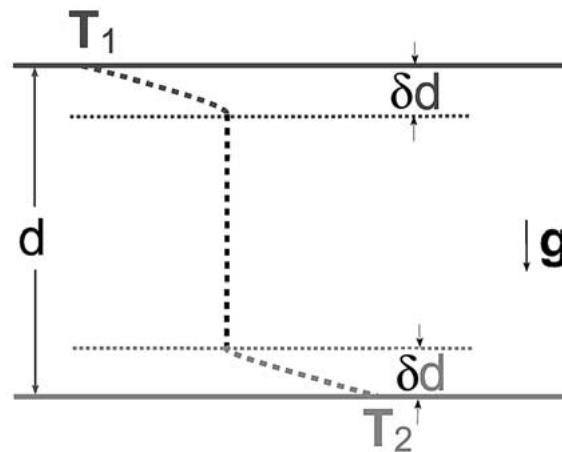


Figure 5. Sketch of the profile of the horizontally averaged temperature in a horizontal fluid layer heated from below.

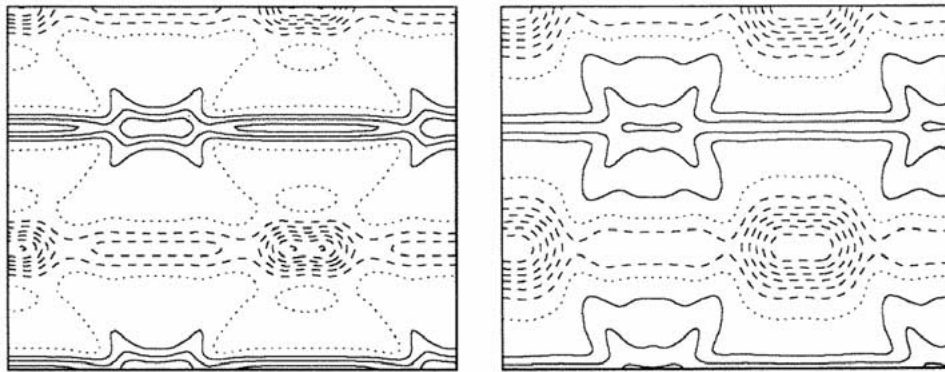


Figure 6. Lines of constant vertical velocity in the plane $z = -0.4$ close to the hot boundary at $z = -0.5$ (left plot) and lines of constant deviations of the negative z -derivative of the temperature from its horizontally averaged value at $z = -0.5$ (right plot). Parameter values are $Ra = 5 \cdot 10^4$, $Pr = 7$, $\alpha_x = 1.6$, $\alpha_y = 2.0$.

wavenumber b along the axis of the rolls. While the three-dimensional patterns evolving from this instability do not differ much from two-dimensional rolls at Rayleigh numbers of the order of 3×10^4 , at higher values of Ra strong plumes evolve along the sheets of ascending and descending fluid. Concurrently streamers evolve in the thermal boundary layers feeding the plumes as shown in Figure 6. These spoke like features look like knots in the shadowgraph observations of convection and have given rise to the name for the instability.

Nearly axisymmetric plumes are more efficient in transporting heat than rolls at not too high Prandtl numbers because of the concentrated upward (downward) momentum with which these plumes impinge on the cold (hot) boundary of the layer, thereby creating strong temperature gradients. While the heat transport by steady

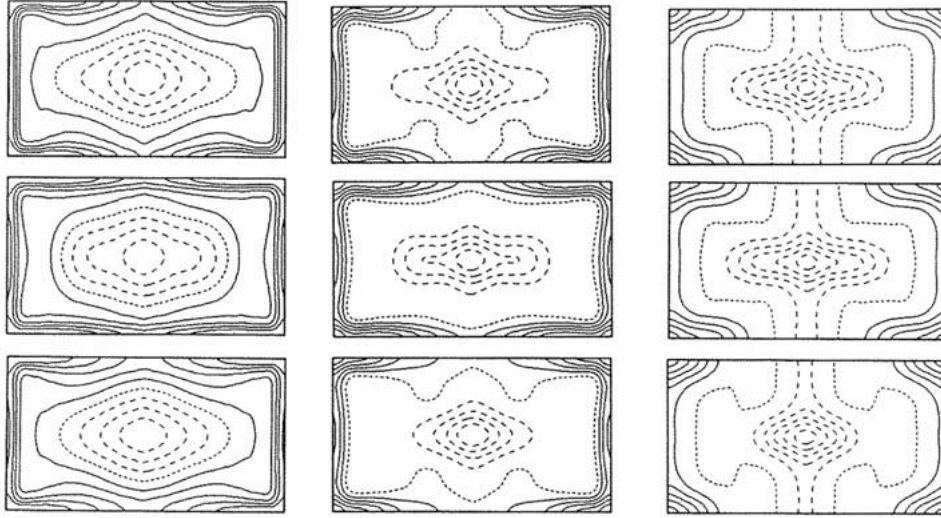


Figure 7. Lines of constant vertical velocity in the midplane of the layer (left column of plots) and in the plane $z = -0.4$ close to the hot boundary at $z = -0.5$ (middle column) and isotherms in the plane $z = -0.4$ for symmetric oscillatory bimodal convection at equally distant times (from top to bottom) such that the fourth picture would repeat the top one. Parameter values are $Ra = 1.4 \cdot 10^5$, $Pr = 60$, $\alpha_x = 4.5$, $\alpha_y = 2.5$.

two-dimensional rolls grows only in proportion to $Ra^{6/5}$, a growth in proportion to $Ra^{4/3}$ appears to be possible in the case of steady knot convection (Clever and Busse, 1989).

The mathematical analysis of tertiary solutions follows in close analogy to the analysis of rolls. After the Galerkin representation

$$X_i = \sum_{l,m,n} a_{lmn}^{(i)} \exp\{il\alpha_x x + im\alpha_y y\} G_n^{(i)}(z) \quad (10)$$

has been introduced, where $\alpha_x = b$, $\alpha_y = \alpha$ have been used, nonlinear algebraic equations for the coefficients $a_{lmn}^{(i)}$ can be obtained by the projection of the basic equations onto the space of the expansion functions used in the representation (10). The algebraic equations can then be solved by a Newton-Raphson method after a suitable truncation of the summations in expression (10) has been employed. By changing the truncation one can ensure that sufficient terms have been taken into account such that a further increase in the number of terms will not change the physically relevant results in any significant way.

Representation (10) is applicable in the case of solutions evolving from instabilities of rolls with $d = 0$ and vanishing value σ_i . But for $\sigma_i \neq 0$ representation (10) can also be used since oscillatory instabilities of rolls typically evolve into traveling waves. In that case x must be replaced by $\hat{x} = x - ct$ and the method of solution proceeds just as in the case of steady tertiary solution. For examples see

TABLE III

Symmetries of twice spatially periodic convection (denoted in terms of the coefficients for the velocity component perpendicular to the boundary)

	Reflection symmetries	Inversion symmetry
Bimodal convection, knot convection	$a_{l-mn} = a_{-lmn} = a_{lmn}$	$a_{lmn} = 0$ for $l + m + n = \text{odd}$
Traveling blob convection	$a_{l-mn} = a_{lmn}$	$a_{lmn} = 0$ for $l + m + n = \text{odd}$
Wavy rolls, wavy Taylor vortices	$a_{lmn} = (-1)^l a_{l-mn} = (-1)^{m+n} a_{-lmn}$	

the work of Clever and Busse (1987, 1989). Even in the case of finite values of d of a growing instability the representation (10) can still be used after $\alpha = \alpha_y$ has been replaced by a fractional value, $\hat{\alpha}_y = \alpha/p$ where the integers p and q are chosen such that $\alpha q/p$ or $\alpha(1 - q/p)$ approximates the values d of the strongest growing disturbances. The evolution of subharmonic instabilities with $d = \alpha/2$ can most easily be analyzed in this way as has been demonstrated, for example, in the work of Nagata and Busse (1983).

Tertiary solutions still exhibit a number of symmetries, in particular in the case when the fluid system obeys the symmetry with respect to the midplane of the layer. The remaining symmetries can be represented most easily by the symmetries of the coefficients $a_{lmn}^{(i)}$. Besides the obvious symmetries $a_{-lmn}^{(i)} = \bar{a}_{lmn}^{(i)}$, $a_{l-mn}^{(i)} = \bar{a}_{l-mn}^{(i)}$ which are required for real expressions of the form (10), several further symmetries are usually found, examples of which are listed in Table III. These symmetries can be profitably employed for a reduction of the computational effort. But they are especially useful for the determination of further symmetry breaking bifurcations. The analysis of the stability of solutions of the form (10) with respect to infinitesimal disturbances is based on the same Equation (4) as in the case of the stability analysis of rolls. Without losing generality we can assume the representation

$$\tilde{X}^{(i)} = \exp\{ibx + idy + \sigma t\} \sum_{lmn} \tilde{a}_{lmn}^{(i)} \exp\{i\alpha_x x + i\alpha_y y\} G^{(i)}(z) \tag{11}$$

for the disturbances with the two Floquet wavenumbers b and d . This ansatz also applies in the case of the traveling waves which are stationary with respect to the coordinate frame \hat{x}, y, z propagating with the phase velocity c in the x -direction. A given tertiary solution characterized by the external parameters as well as by the two wavenumbers α_x, α_y is found to be stable with respect to infinitesimal disturbances if there does not exist a growth rate σ as a function of the parameters b and d with a positive real part σ_r . Otherwise the tertiary solution is unstable. Of course, there are again the obvious solutions, $\tilde{X} = \frac{\partial}{\partial x} X$, $\tilde{X} = \frac{\partial}{\partial y} X$ of Equation

(4) with $\sigma = b = d = 0$ which correspond to shifts of the tertiary solution in the x, y -plane. The most important instabilities also share the property $b = d = 0$, at least within a restricted region of the α_x - α_y -parameter space. Often they introduce a time dependence which no longer can lead to a purely propagating wave since there is no homogeneous spatial direction available anymore. Thus standing oscillations must typically be expected. Such solutions can be represented in the form (10) if another expansion in terms of Fourier modes $\exp\{ik\omega t\}$, $k = 0, 1, \dots$, is added. But usually it is simpler to allow for time dependent coefficients $a_{lmn}^{(i)}(t)$. Instead of the nonlinear algebraic equations for the $a_{lmn}^{(i)}$ a system of ordinary nonlinear differential equations in time is then obtained which can be solved by numerical integration after a suitable truncation has been introduced. The only disadvantage of this latter method is that further bifurcations involving the breaking of the periodicity in time may not easily be detected. But bifurcations with broken spatial symmetries can still be identified when the coefficients $a_{lmn}^{(i)}(t)$ which are supposed to vanish begin to grow in time.

According to the procedures outlined in this section it is clear that bifurcations can be found as long as there are symmetries left which can be broken. But because of the rapidly increasing numerical effort required for a complete stability analysis it will usually not be possible to investigate all possible bifurcation branches. Even if solutions are already unstable to some long wavelength modulations it may still be profitable to search for short wavelength instabilities which introduce new transport mechanisms. In this sense the sequence-of-bifurcations approach can be useful even in the case of unstable solutions.

5. Oscillatory Bimodal Convection as an Example of a Quaternary Solution

Using controlled initial conditions experimenters can easily realize steady spatially periodic flows representing bimodal convection in the laboratory (Krishnamurti 1970; Busse and Whitehead, 1971). A tertiary bifurcation leads to oscillatory bimodal convection at moderate Prandtl number of the order 10^2 which also has been realized in the laboratory (Busse and Whitehead, 1974). There are actually two oscillatory instabilities of steady bimodal cells, one that does not change the spatial symmetry and is thus called the symmetric oscillatory instability and the wavy oscillatory instability, which breaks the reflection symmetry of the superimposed small wavelength rolls. The former is preferred at somewhat higher Prandtl numbers than the latter which will occur primarily in the regime $10 \lesssim Pr \lesssim 50$. But a detailed analysis shows that the wavenumbers α_x, α_y of the steady bimodal solutions also exert a strong influence on the mechanism of instability (Clever and Busse, 1994).

An impression of the symmetric oscillatory instability is given by Figures 7, and 8. As can best be seen in the plots of the vertical velocity at $z = -0.4$ close to the lower boundary ($z = -0.5$) in Figure 7, the flow in the secondary cross rolls

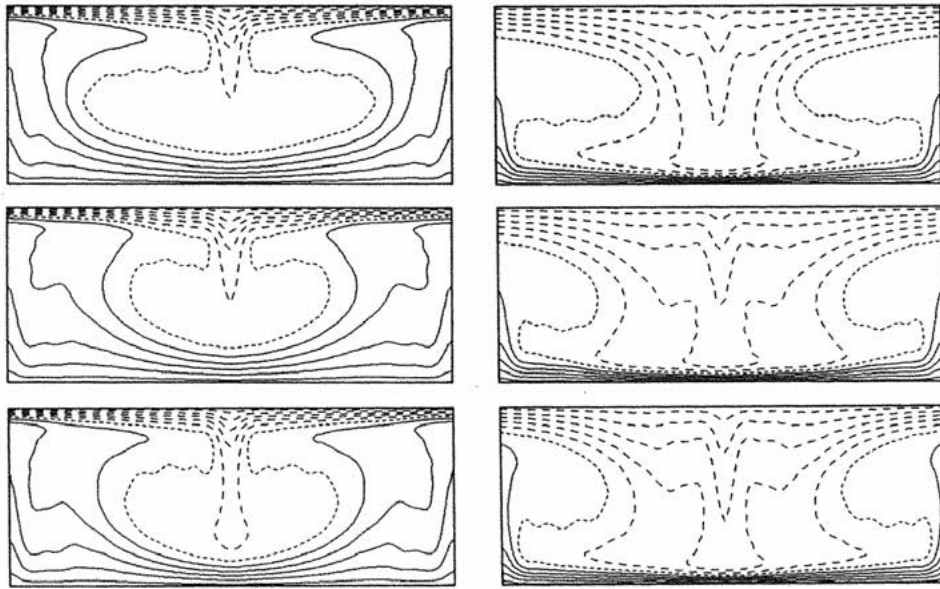


Figure 8. Isotherms in the planes $x = 0$ (left column) and $x = \pi/\alpha_x$ (right column) for the same case as Figure 7.

periodically contracts towards and expands from the points of intersection with the primary rolls. This “breathing” is associated with alternating hotter and colder than average fluid circulating around the convection cell as indicated in Figure 8. This process is similar to the periodic boundary layer instability proposed by Howard (1966), but the period of the oscillations is given by the circulation time in the bimodal cell. Oscillations associated with traveling hot and cold blobs can also occur as an instability of two-dimensional convection rolls (Bolton et al., 1986) and their properties have been investigated by Clever and Busse (1995).

The wavy oscillatory instability exhibits the additional feature that the up- and down-moving sections of the secondary cross rolls shift their position back and forth in the direction along the axis of the primary rolls as indicated in Figure 9. Since the shift occurs in opposite directions in the upper and lower halves of the layer, the shadowgraph image of the experimental observation seems to indicate a splitting of the boundary of the secondary rolls at the phase of maximum amplitude as shown in Figure 10. While the experimentally realized oscillatory bimodal convection is nearly spatially and temporally periodic, the phase of oscillation exhibits large scale modulations as is evident from the figure. This feature has not yet been explored in any theoretical analysis.

With increasing Rayleigh number a subharmonic instability with a typical new wavenumber $\tilde{\alpha}_x = \alpha_x/3$ (Clever and Busse, 1994) leads to a destruction of the oscillatory bimodal cells and introduces a larger scale pattern as shown in Figure 11. This type of convection is essentially the same as oscillatory knot convection

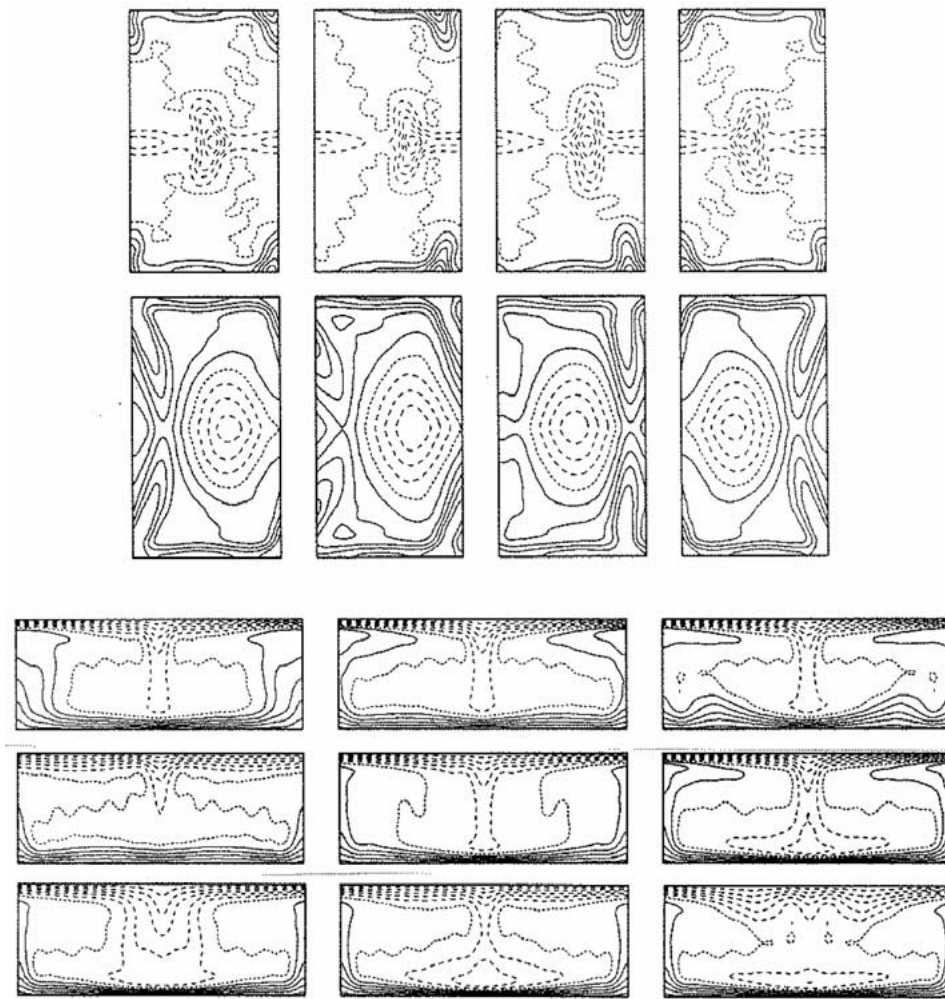


Figure 9. The upper part shows isotherms for wavy oscillatory bimodal convection in the middle plane $z = 0$ (uppermost row) and in the plane $z = -0.4$ close to the lower boundary at $z = -0.5$ (second row) at the times $t = n\pi/3\omega$ for $n = 0, 1, 2, 3$ (left to right) such that half a period of oscillation has passed between the first and the last picture. The lower part of the figure shows isotherms at the y, z -planes $x = 0, x = \pi/2\alpha_x$ and $x = \pi/\alpha_x$ (from top to bottom) at the times $t = n\pi/3\omega$ for $n = 0, 1, 2$. In the lower part of the figure y increases towards the right and z increases upwards while in the upper part x increases towards the right and y increases upwards. The parameter values $Pr = 30, Ra = 10^5, \alpha_x = 4.5, \alpha_y = 2.5$ have been used.

(Clever and Busse, 1989). While the large scale structure remains nearly steady, the hot and cold streamers in the respective thermal boundary layers are strongly time dependent. In experiments starting with random initial conditions, the same structures of large scale nearly steady cells coexisting with turbulent small scale motions originating from the unstable thermal boundary layers can be seen, except

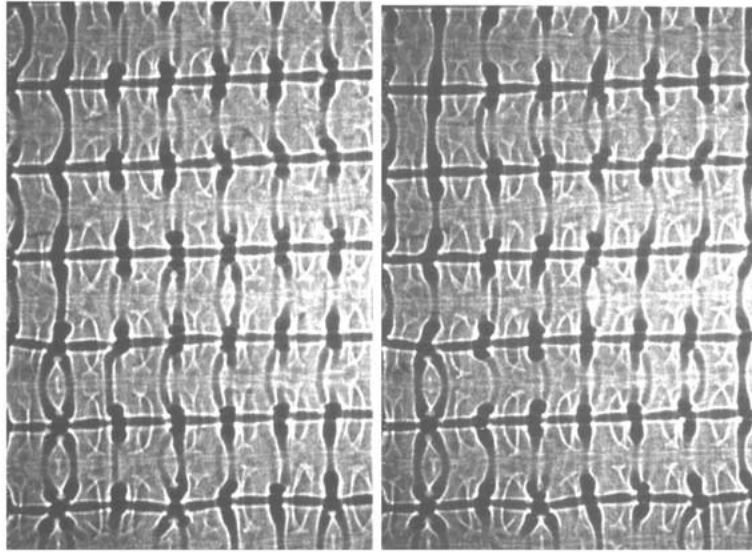


Figure 10. Shadowgraph observation of wavy oscillatory bimodal convection in a layer of silicon oil heated from below. The dark regions indicate hot rising fluid. The Prandtl and Rayleigh numbers are $Pr = 63$, $Ra = 1.5 \cdot 10^5$ and the wave numbers in the x -direction (towards the right) and y -direction are given by $\alpha_x = 4.08$, $\alpha_y = 2.04$. The right photograph has been taken 25 sec. after the left one which corresponds to nearly half a period. For details see Busse and Whitehead (1974).

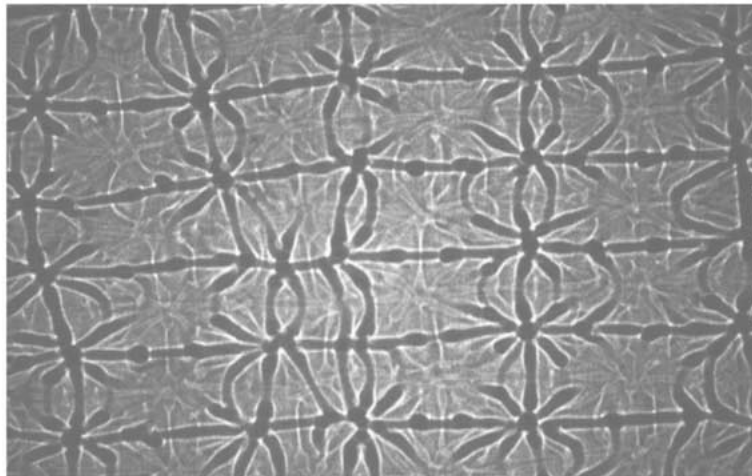


Figure 11. Shadowgraph observation of spoke pattern convection in a layer of silicon oil heated from below. The experimental parameters are the same as in Figure 10 except that the Rayleigh number is slightly higher.

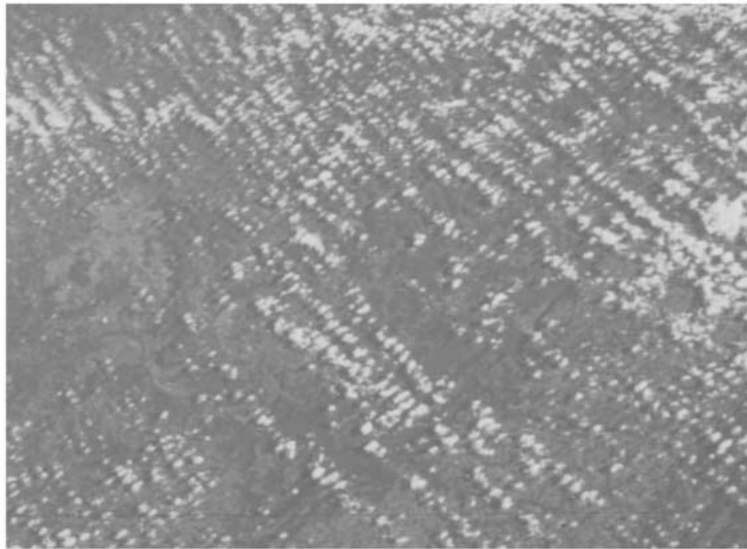


Figure 12. Photograph of cloud streets as seen from above.

that now the cells are approximately squares since any memory of the original roll convection is lost (Busse, 1994).

6. Discussion

Atmospheric scientists are familiar with regular structures in highly turbulent systems since clouds serve as convenient indicators for many convective processes in the atmosphere. The regularly spaced cloud streets indicate the alignment of convection rolls with the shear of the mean wind and pictures taken by satellites have made us aware of the regular patterns of “open” and “closed” cells with hexagonal shape in mesoscale convection. Here I wish to draw attention to the fact that tertiary forms of convection such as bimodal cells may also be seen in cloud patterns. As shown in Figure 12 the clouds aligned like pearls on a string in some cloud streets can exhibit the typical form of bimodal convection with a wavelength of the secondary roll in the direction of the street which is much smaller than the basic wavelength of the cloud street. That convection in the atmosphere may show typical phenomena of high Prandtl number fluids is not surprising when the effect of latent heat release in clouds is considered. Because of the strong increase of the heat capacity of moist air in connection with the condensation of water vapor, the effective thermal diffusivity is strongly diminished and the Prandtl number is thus increased. Different three-dimensional structures superimposed onto convection rolls are indeed observed in clear air as found by Markson (1975) which may indicate the wavy rolls expected for $Pr = 0.7$ (Clever et al., 1977).

The fact that clouds in the atmosphere or the shadowgraph method in laboratory experiments provide an instantaneous two-dimensional image of the turbulent system is one of the reasons that more regular structures are observed in turbulent convection than in other turbulent fluid systems. Moreover, there are no mean flows or only weak ones which would carry the turbulent structure out of the observational frame before it has a chance to evolve. It thus seems likely that the sequence-of-bifurcation approach could find many applications beyond problems of convection once appropriate methods of observations have been developed. In the Taylor-Couette system, transitions to more complex forms of fluid flow can still be observed fairly easily and maps of different states of flow have been produced (Andereck et al., 1986). But the analysis of bifurcation sequences has not yet proceeded far enough to explain all the different states. For a discussion of the possible symmetries of the states of flow we refer to Crawford and Knobloch (1991) and Chossat and Iooss (1994).

There is no direct connection, however, between symmetries and physical mechanism giving rise to bifurcations. When the bifurcation sequence depends on additional parameters besides the control parameter R (such as the Prandtl number in the case of Rayleigh-Bénard convection) it is often found that typical dynamical mechanisms may enter earlier or later in the sequence of bifurcations under conditions of quite different symmetries. We thus find that the oscillatory blob convection (Clever and Busse, 1995) is realized as a tertiary solution or as quaternary solutions in the form of oscillatory knot convection or oscillatory bimodal convection. This is another indication for the robustness of mechanisms which, not surprisingly, also operate in the turbulent state.

References

- Andereck, C. D., Liu, S. S., and Swinney, H. L.: 1986, Flow regimes in a circular Couette system with independently rotating cylinders, *J. Fluid Mech.* **164**, 155–183.
- Bolton, E. W. and Busse, F. H.: 1985, Stability of convection rolls in a layer with stress-free boundaries, *J. Fluid Mech.* **150**, 487–498.
- Bolton, E. W., Busse, F. H., and Clever, R. M.: 1986, Oscillatory instabilities of convection rolls at intermediate Prandtl numbers, *J. Fluid Mech.* **164**, 469–485.
- Brown, G. L. and Roshko, A.: 1974, On density effects and large structure in turbulent mixing layers, *J. Fluid Mech.* **64**, 775–816.
- Busse, F. H.: 1967a, The stability of finite amplitude cellular convection and its relation to an extremum principle, *J. Fluid Mech.* **30**, 625–649.
- Busse, F. H.: 1967b, On the stability of two-dimensional convection in a layer heated from below, *J. Math. Phys.* **46**, 140–150.
- Busse, F. H.: 1994, Spoke pattern convection, *Acta Mechanica (Suppl.)* **4**, 11–17.
- Busse, F. H. and Clever, R. M.: 1979, Instabilities of convection rolls in a fluid of moderate Prandtl number, *J. Fluid Mech.* **91**, 319–335.
- Busse, F. H. and Whitehead, J. A.: 1971, Instabilities of convection rolls in a high Prandtl number fluid, *J. Fluid Mech.* **47**, 305–230.

- Busse, F. H. and Whitehead, J. A.: 1974, Oscillatory and collective instabilities in large Prandtl number convection, *J. Fluid Mech.* **66**, 67–79.
- Chossat, P. and Iooss, G.: 1994, *The Couette-Taylor problem*, *Appl. Math. Sci.*, vol. 102, Springer.
- Clever, R. M. and Busse, F. H.: 1974, Transition to time-dependent convection, *J. Fluid Mech.* **65**, 625–645.
- Clever, R. M., Busse, F. H., and Kelly, R. E.: 1977, Instabilities of longitudinal convection rolls in couette flow, *J. Appl. Math. Phys. (ZAMP)* **28**, 771–783.
- Clever, R. M. and Busse, F. H.: 1987, Nonlinear oscillatory convection, *J. Fluid Mech.* **176**, 403–417.
- Clever, R. M. and Busse, F. H.: 1989, Three-dimensional knot convection in a layer heated from below, *J. Fluid Mech.* **198**, 345–363.
- Clever, R. M. and Busse, F. H.: 1989, Nonlinear oscillatory convection in the presence of a vertical magnetic field, *J. Fluid Mech.* **201**, 507–523.
- Clever, R. M. and Busse, F. H.: 1994, Steady and oscillatory bimodal convection, *J. Fluid Mech.* **271**, 103–118.
- Clever, R. M. and Busse, F. H.: 1995, Standing and traveling oscillatory blob convection, *J. Fluid Mech.* **297**, 255–273.
- Crawford, J. D. and Knobloch, E.: 1991, Symmetry and symmetry-breaking bifurcations in fluid dynamics, *Ann. Rev. Fluid Mech.* **23**, 341–87.
- Frick, H., Busse, F. H., and Clever, R. M.: 1983, Steady three-dimensional convection at high Prandtl number, *J. Fluid Mech.* **127**, 141–153.
- Krishnamurti, R.: 1970, On the transition to turbulent convection. Part 1. The transition from two to three-dimensional flow, *J. Fluid Mech.* **42**, 295–307.
- Markson, R.: 1975, Atmospheric electrical detection of organized convection, *Science* **188**, 1171–1177.
- Nagata, M. and Busse, F. H.: 1983, Three-dimensional tertiary motions in a plane shear layer, *J. Fluid Mech.* **135**, 1–26.
- Schlüter, A., Lortz, D., and Busse, F. H.: 1965, On the stability of steady finite amplitude convection, *J. Fluid Mech.* **23**, 129–144.